Journal of Electrochemistry

Volume 22
Issue 2 *Special issue of Electrocatalyst and Electrocatalysis in Fuel Cells(Editor: Professor WEI Zi-dong)*

2016-04-28

Nitrogen, Fluorine co-doped Silk-derived Carbon for Electrochemical Oxygen Reduction with High Performance in Alkaline Solution

Fang-fang LIU

Hong-liang PENG

Shi-jun LIAO
ey Lab for Fuel Cell Technology of Guangdong Province & Key Lab of New Energy Technology of Guangdong Universities, School of Chemistry and Chemical Engineering, South China University of Technology, Guangzhou, 510641, China;, chsjliao@scut.edu.cn

Recommended Citation
Fang-fang LIU, Hong-liang PENG, Shi-jun LIAO. Nitrogen, Fluorine co-doped Silk-derived Carbon for Electrochemical Oxygen Reduction with High Performance in Alkaline Solution[J]. *Journal of Electrochemistry*, 2016 , 22(2): 151241.
DOI: 10.13208/j.electrochem.151141
Available at: https://jelectrochem.xmu.edu.cn/journal/vol22/iss2/14

DOI: 10.13208/j.electrochem.151141 **Artical ID**:1006-3471(2016)02-0164-12
Cite this: *J. Electrochem.* **2016**, *22*(2): 164-175 **Http**://electrochem.xmu.edu.cn

Nitrogen, Fluorine Co-Doped Silk-Derived Carbon for Electrochemical Oxygen Reduction with High Performance in Alkaline Solution

LIU Fang-fang[1,2], PENG Hong-liang[1], LIAO Shi-jun[1*]
(1. *Key Lab for Fuel Cell Technology of Guangdong Province & Key Lab of New Energy Technology of Guangdong Universities, School of Chemistry and Chemical Engineering, South China University of Technology, Guangzhou*, 510641, *China*; 2. *School of Chemical Engineering and Environment, Weifang Univesity of Science and Technology, Shouguang, Shandong*, 262700, *China*)

Abstract: A high-performance, doped carbon-based catalyst was synthesized by pyrolyzing hydrothermally treated silkworm cocoon. The effects of preparation conditions and fluorine promotion on various catalysts' performance were investigated. The catalyst prepared under optimal conditions and doped with nitrogen and fluorine possessed the high specific surface area of more than 1000 $m^2 \cdot g^{-1}$ and contained 3.5 and 7.3%(by mass, the same below) N and F, respectively. The activity of the catalyst toward oxygen reduction reaction in an alkaline medium was comparable to that of commercial Pt/C, showing both superior tolerance to methanol poisoning and better durability. Doping with fluorine was found to significantly enhance the performance of catalyst. Possible mechanism for the addition of fluorine is suggested.

Key words: biomass-derived; oxygen reduction reaction; carbon materials; nitrogen; fluorine co-doping
CLC Number: O646, TM911.46 **Document Code**: A

Fuel cells are highly promising clean energy generation devices, and electrocatalysts play a key role in the oxygen reduction reaction (ORR) at their cathode[1-5]. Platinum (Pt) and its alloys have long been regarded as the most effective catalysts for the ORR in fuel cells. However, it is generally accepted that the large-scale production and application of fuel cells using Pt-based electrocatalysts are not commercially viable due to the scarcity and high price of Pt. These catalysts also have other major drawbacks, including significant intolerance of intermediates, anode crossover, sluggish kinetics, and poor stability in an electrochemical environment[6-7]. Hence, the development of highly efficient, inexpensive, and readily available ORR electrocatalysts to replace Pt-based ones is paramount for the future of fuel cell technology.

To date, amongst the various metal-free ORR electrocatalysts that have been investigated[8-10], heteroatom-doped carbon materials are widely recognized as a promising class of candidates. A number of different approaches have been employed to dope heteroatoms into carbon structures (e.g., high-temperature carbonization of heteroatom containing precursors, high-temperature post-treatment, and hydrothermal treatment of heteroatom-containing precursors) [11-26]. However, these approaches either involve tedious and complex experimental procedures, or require harsh reaction conditions and have low production

Received: 2015-11-26, Revised: 2015-12-18 *Corresponding author, Tel: (86-20)87113586, E-mail: chsjliao@scut.edu.cn
This work was supported by the National Science Foundation of China(NSFC Project Nos. 21076089, 21276098, 11132004, and U1301245), the Ministry of Science and Technology of China (Project No. 2012AA053402), the Guangdong Natural Science Foundation (Project No. S2012020011061), the Doctoral Fund of the Ministry of Education of China (20110172110012), and the Basic Scientific Foundation of the Central Universities of China (No. 2013ZP0013).

yields. They almost exclusively require the uses of synthetic chemicals as carbon and heteroatom sources.

It is, therefore, highly desirable to achieve heteroatom doping using simple, low-cost, high-yield, and environmentally friendly synthesis methods to fabricate commercially viable carbon-based materials that can replace Pt-based electrocatalysts for the ORR. Carbon materials derived from biomass have been receiving considerable attention because biomass is recyclable and extensively available. Generally, in addition to containing carbon and water, biomass is rich in sulfur, nitrogen, and phosphorus, as well as certain metals, including Fe and Cu. Some researchers have investigated these new types of doped carbon materials prepared by pyrolyzing biomass, but to date, only a few of the resulting catalysts have been active toward the ORR[27-43]. Gao et al. reported a N-doped porous carbon catalyst fabricated using fermented rice as the starting material and activated by $ZnCl_2$. They found that the as-prepared catalyst was r esistant to the methanol crossover effects and CO poisoning, and demonstrated a level of ORR activity[40]. Chen et al. synthesized the N-doped nanoporous carbon nanosheets by pyrolyzing the plant Typha orientalis (a type of bullrush) in NH_3 after hydrothermal treatment. The product exhibited similar catalytic activity to that of commercial 20% Pt/C in an alkaline medium, as well superior methanol tolerance[39].

Silk is a natural protein fiber obtained from a silkworm through an artificial electrospinning-like process, in which the silkworm spins silk microfibers to form a cocoon around itself[44]. The silk cocoon con tains a considerable amount of nitrogen (16.2%) because its chemical structure is mainly characterized by the presence of 18 types of amino acids, such as glycine, alanine, and serine[34, 44]. Therefore, it is not surprising that silk cocoon also has a significant amount of nitrogen-containing functional groups. We speculated that the introduction of this high nitrogen-containing material as a precursor would boost the resulting material's performance.

Herein, we present an easy, green strategy to synthesize a new type of N-doped, non-precious metal electrocatalyst by using raw silk cocoon as the precursor for carbon and nitrogen, and using fluorine-containing polytetrafluoroethylene (PTFE) powder as an effective promoter. The natural cocoon microfibers were directly transformed into 1D carbon microfibers. This new type of electrocatalyst exhibited not only excellent electrocatalytic activity toward the ORR, but also superior stability compared with commercial carbon-supported Pt, thus, offering a new high-performance catalyst for the ORR.

1 Experimental

1.1 Preparation of Doped Carbonaceous Composite Materials

The typical catalyst synthesis procedure was as follows. First, 3.0 g silkworm cocoon and 30 mL distilled water were placed in an autoclave at 180 ℃ for 12 h, yielding a yellow-brown carbonaceous hydrogel. Second, a carbonaceous aerogel was obtained by drying the hydrogel for 24 h. Finally, F and N co-doped carbon catalysts (SWF-*n*/*m*) were prepared by pyrolyzing a mixture of the aerogel and PTFE powder in an Ar atmosphere at 900 ℃ for 2 h, followed by leaching in 1 mol·L^{-1} H_2SO_4 at 80 ℃ for 8 h, and annealing at 900 ℃ for another 1 h under Ar flow, where n/m refers to the mass ratio of the aerogel of silkworm cocoon and PTFE powder.

For comparison, a silkworm-derived doped carbon catalyst was prepared by using the same procedures but without the addition of PTFE, which is named as SW.

1.2 Physical Characterization

X-ray diffraction (XRD) test was conducted on a TD-3500 powder diffractometer (Tongda, China). Specific surface areas and pore-size distributions were measured by Brunauer-Emmett-Teller (BET) nitrogen adsorption-desorption at 77 K on a Tristar II 3020 gas adsorption analyzer (Micromeritics, USA). Scanning electron microscopy (SEM) observations were conducted on a Nova Nano 430 field emission scanning electron microscope (FEI, Netherlands). Transmission electron microscopy (TEM) images were recorded on a JEM-2100 transmission electron microscope (JEOL,

Japan). Raman spectroscopic measurement was performed on a LabRAM Aramis Raman spectrometer (HJY, France) with a laser wavelength of 632 nm. X-ray photoelectron spectroscopy (XPS) analysis was performed on an ESCALAB 250 X-ray photoelectron spectrometer (Thermo-VG Scientific, USA). Analysis of carbonyl bridges was carried out on a Bruker Equinox 55 Fourier transform infrared (FTIR) spectrometer. Elemental analysis was performed on a Vario Micro setup (Elementar Analysensysteme GmbH, Germany) to determine the sulfur, carbon, nitrogen, and hydrogen contents.

1.3 Electrochemical Measurement

Electrochemical measurements were conducted in a standard three-electrode glass cell on an electrochemical workstation (Ivium, Netherlands) at room temperature, coupled with a rotating disk electrode (RDE) system (Pine Research Instrumentation, USA). A glassy carbon electrode (GCE, with a diameter of 5 mm and an electrode area of 0.1964 cm^2) was used as the working electrode substrate, with Ag/AgCl (3 $mol \cdot L^{-1}$ KCl) and Pt wire as the reference electrode and counter electrode, respectively. For simplicity, we calibrated the Ag/AgCl (3 $mol \cdot L^{-1}$ KCl) reference electrode, and all potentials in this paper are reported with respect to a reversible hydrogen electrode (RHE). The potential difference between the RHE and the Ag/AgCl electrode in the alkaline electrolyte was 0.982 V.

Koutecky-Levich (K-L) plots were obtained by linear fitting of the reciprocal rotating speed versus the reciprocal current density collected at different potentials from 0.78 to 0.48 V. The transferred electron number per O_2 involved in oxygen reduction was determined by the following K-L equation:

$$J^{-1} = J_L^{-1} + J_K^{-1} = B^{-1}\omega^{-1/2} + J_K^{-1} \quad (1)$$

where J is the measured current, J_K is the kinetic-limiting current, and ω is the electrode rotation rate. The theoretical value of the Levich slope (B) is evaluated from the following relationship:

$$B = 0.62nFC_0D_0^{2/3}\upsilon^{-1/6} \quad (2)$$

where n is the overall number of transferred electrons in the ORR process, F is the Faradaic constant (96485 $C \cdot mol^{-1}$), C_0 is the oxygen concentration (solubility) in 0.1 $mol \cdot L^{-1}$ KOH (1.2×10^{-6} $mol \cdot cm^{-3}$), and D_0 is the oxygen diffusion coefficient in 0.1 $mol \cdot L^{-1}$ KOH.

Before every measurement, the GCE surface was cleaned by ultrasonication in ethanol and polished with an Al_2O_3 slurry (50 nm) on a microcloth, followed by rinsing with deionized water and drying under an infrared lamp. Slurry of the active material was prepared by mixing under ultrasonication 5.0 mg catalyst with 1 mL ethanol solution containing Nafion (0.25%). Next, 20 mL catalyst slurry was pipetted onto the surface of the GCE, followed by drying under an infrared lamp to form a catalyst film on the GCE substrate. The catalyst loading was approximately 0.51 $mg \cdot cm^{-2}$. Linear sweep voltammetry (LSV) measurements were conducted in 0.1 $mol \cdot L^{-1}$ KOH solution at a scan rate of 10 $mV \cdot s^{-1}$. The LSV curves were recorded at a disk rotation rate ranging from 1600 to 3600 $r \cdot min^{-1}$. Before every measurement, the KOH solution was saturated with pure N_2 (99.999%) or pure O_2 (99.999%) for at least 30 min. All the current densities were normalized to the geometric area of the GCE. The chronoamperometric response was obtained at 0.68 V (vs. RHE) in an O_2-saturated electrolyte. 2.0 mL mixed solutions (0.1 $mol \cdot L^{-1}$ KOH + 3 $mol \cdot L^{-1}$ methanol) into the electrolyte after about 200 s (the test was paused 2 min to mix the solution uniform) to examine the methanol crossover. We also conducted a durability testing of the catalyst for 25,000 s at 0.68 V in O_2-saturated 0.1 $mol \cdot L^{-1}$ KOH solution using the same setup and a scanning rate of 10 $mV \cdot s^{-1}$ at 900 $r \cdot min^{-1}$.

2 Results and Discussion

Fig. 1 shows the representative SEM images of a raw silkworm cocoon (A), the N-doped carbon catalyst derived from the silk material (SW) (B), and the N and F co-doped carbon catalyst (SWF-1/4) derived from the mixture of silk and PTFE (C). These images illustrate that the SW was made up of many uniform 1D carbon microfibers with an average diameter of 6 μm [44]. It is important to note that the microfiber structure was mostly destroyed after the addition of

PTFE and, therefore, was no longer uniform (Fig. 1C). This may have been caused by fluorination due to the PTFE. Fig. 1D gives a scanning TEM image of the SWF-1/4, clearly displaying its porous structure, which was confirmed by the nitrogen adsorption-desorption results to be seen below.

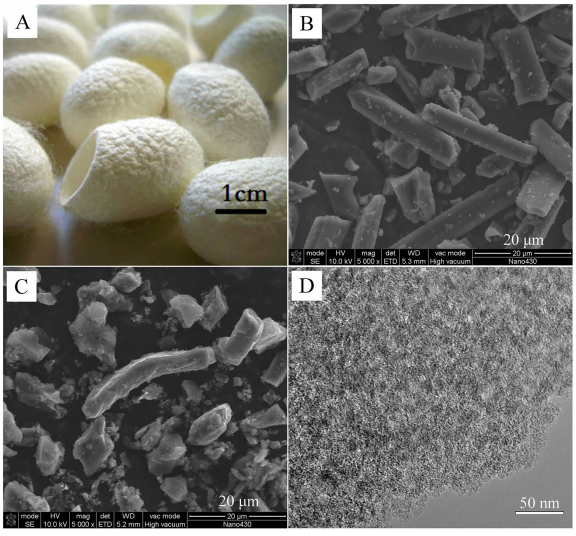

Fig. 1 SEM images of a raw silk cocoon (A), SW (B), and SWF-1/4 (C); D. TEM image of SWF-1/4

Fig. 2 presents the XRD patterns of the SW sample and a series of SWF samples doped with various amounts of fluorine. Two characteristic peaks located at 2θ values of 25° and 44° are attributable to the (002) and (101) diffraction peaks of graphitic carbon, respectively. All of the samples might initially appear to have almost the same XRD patterns; however, there is in fact a clear negative shift in the peaks of the samples containing PTFE-and the shift increases with the amount of PTFE. Our previous research [45] has found the same interesting result that the addition of fluorine into nitrogenous substances increases the d-spacing of the (002) crystal planes (i.e., the interlayer distance). However, its specific mechanism has not been fully understood and is worth the further research in our next work.

Fig. 3 displays the XPS spectra for the SW and N, F co-doped SWF-1/4 samples. The peak for the C═C bond, located at 284.8 eV, is dominant in both samples. As Fig. s. 3A and 3B show, both SW and

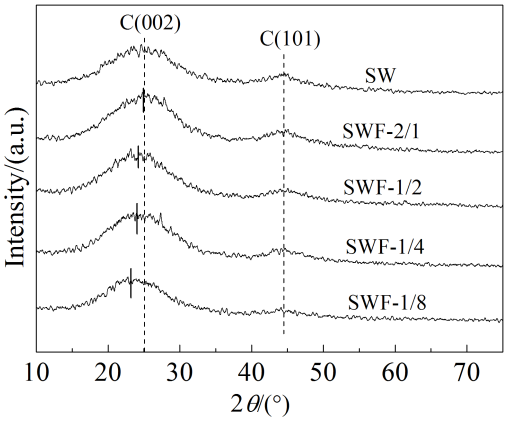

Fig. 2 XRD patterns of SW and SWF samples pyrolyzed at 900 °C

SWF-1/4 samples possessed almost the same amounts of N content (ca. 3.0 ~ 3.5%), while the latter had the lower O content. Calculations determined that the N, F co-doped sample contained about 7.3% F. A weak peak centered at 291.8 eV (Fig. 3C, D) is attributable to the semi-ionic C—F bond [46-47]. The high-resolution N1s spectra of SW and SWF-1/4 (Fig. 3E, F) can both be further deconvoluted into four different signals with binding energies of 398.5, 400.0, 401.0, and 402.0 eV, corresponding to pyridinic-N[48], pyrrolic-N, graphitic-N[49], and oxidized-N[50-51], respectively. As shown in the insets, the percentages of these different N species were 25.2, 24.6, 23.0, and 27.3% (by atom) for the former and 27.1, 14.5, 39.6, and 18.8% (by atom) for the latter. Generally, of the first three species, pyridinic-N is recognized as particularly active because it has a lone electron pair in the plane of the carbon matrix, which increases the catalyst's ability to donate electrons. Significant amounts of these active N species (which include pyrrolic and graphitic as well as pyridinic N) can induce better catalytic performance. Clearly, the N, F co-doped catalyst (SWF) had a higher proportion of active N species, even though its total N content was almost the same as that of SW.

In addition, as shown in Fig. 3G, an obvious F1s core-level peak appears at 689.2 eV. According to the literature[46-47], this is attributable to F with ionic characteristics, implying the transfer of electrons from neighbouring carbon atoms to F atoms. Its presence

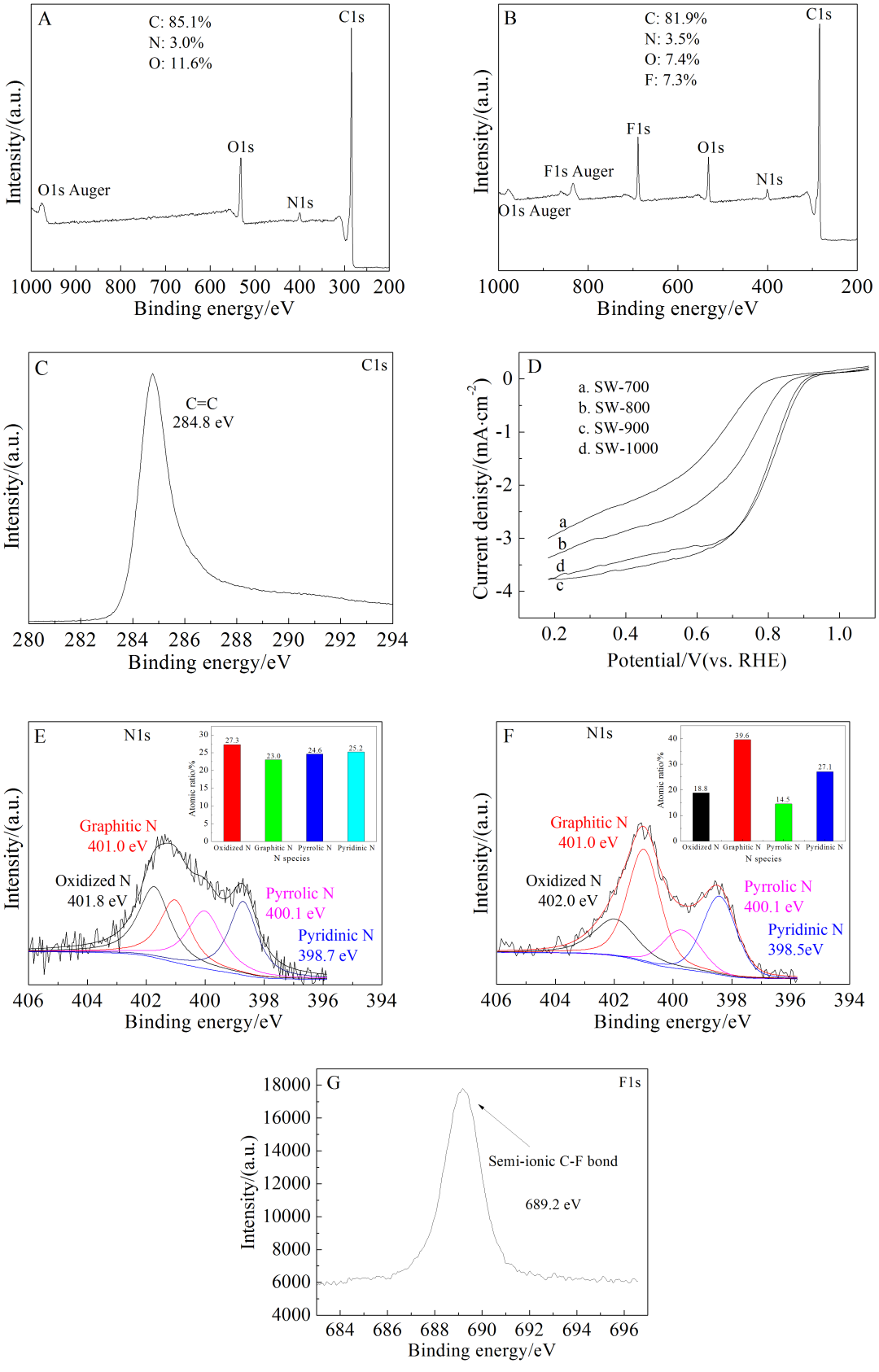

Fig. 3 A-B. XPS survey spectra of SW and SWF-1/4; C-D. High-resolution C1s XPS spectra of SW and SWF-1/4; E-F. High-resolution N1s XPS spectra of SW and SWF-1/4 (the insets: charts showing the percentages for different types of nitrogen); G. High-resolution F1s XPS spectra of SWF-1/4

would, therefore, be beneficial in the formation of active centers for the ORR and would enhance the catalyst's performance.

Fig. 4 shows the Raman spectra of different samples. The peaks at ~ 1320 and ~ 1580 cm^{-1} can be assigned to the D and G bands of carbon, respectively. Generally, the D-band peak originates from lattice distortion due to sp^2-defects (e.g., vacancy, topological defects, and impurities), and the G-band peak results from the E_{2g} vibrational mode in the $D4_{6h}$ symmetry group of the graphite crystal planes[52]. Therefore, the ratio of the D-band and G-band intensities (I_D/I_G) is commonly considered as an indication for the extent of the defects in a doped carbon catalyst[53]. As shown in Fig. 4, the I_D/I_G ratio is 1.35 for SW, and 1.45, 1.47, 1.56, and 1.62 for SWF-2/1, SWF-1/2, SWF-1/4, and SWF-1/8, respectively. Clearly, the defect sites (i.e., the edge planes) increased with the amount of doped F[20], resulting in higher ORR performance.

FTIR spectrometry was used to characterize the materials. We found that after hydrothermal treatment, the raw biomass gel contained large amounts of C—O—C (900 ~ 1100 cm^{-1}), C—O (1000 ~ 1300 cm^{-1}), benzene C═C or N—H (1500~1620 cm^{-1}), —CH_3 (1300 ~ 1500 cm^{-1}), and —CH_2 (2850 ~ 3000 cm^{-1}) bonds[54-55] (Fig. 5A), reflecting the composition of the silk protein (amino acids) in the silkworm cocoon.

After the materials were pyrolyzed at 900 ℃, their FTIR spectra changed significantly, demonstrating that the internal structure of the biomass altered during high-temperature pyrolysis. A major decrease

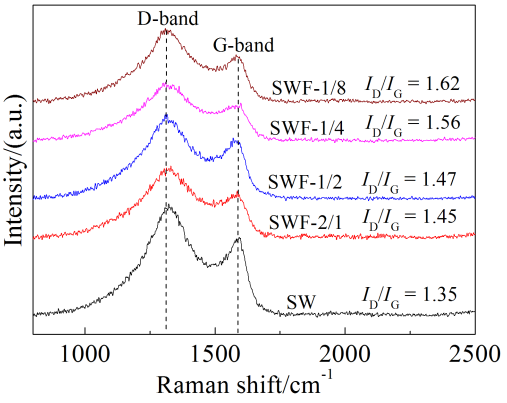

Fig. 4 Raman spectra of different samples

in the relative intensities of the aforementioned resonances was observed, indicating the decomposition of the silkworm cocoon-derived degradation/hydrolysis products. In the samples doped with PTFE, a C—F bond at 1100 ~ 1300 cm^{-1} was observed[56]; after the addition of PTFE, the peak shifted slightly, confirming the successful doping of the sample with fluorine.

Elemental analysis was used to measure the amounts of C, N, and S in the catalysts (Tab. 1). The N content of sample SW was about 3%, far below that of raw silk, which may have been due to the decomposition and volatilization of nitrogenous substances during the hydrothermal treatment and pyrolysis process. The addition of PTFE slightly influenced the N content of catalysts. When the ratio of aerogel to PTFE reached 1:4, the catalyst exhibited the highest N content (3.8%) and the lowest S content (0.3%). Interestingly, this catalyst exhibited the highest ORR activity, indicating that N content may have been one

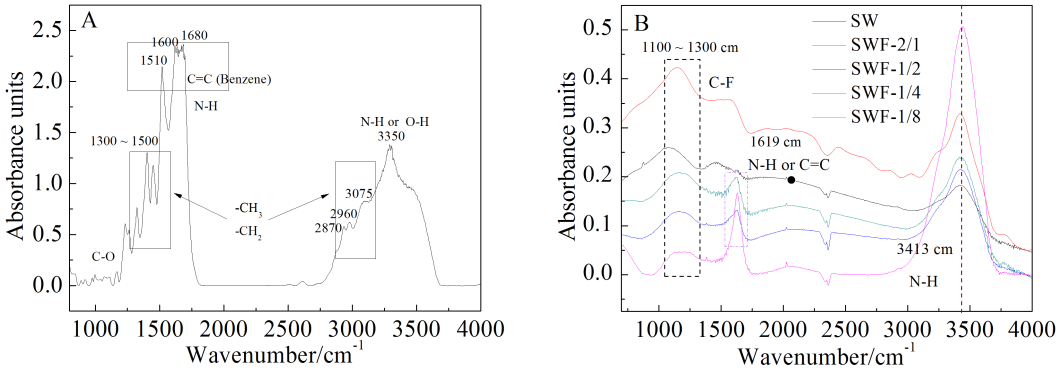

Fig. 5 FTIR spectra of raw biomass after hydrothermal treatment (A) and samples after pyrolysis (B)

Tab. 1 Elemental analysis results of the different samples

Sample	N%	C%	H%	S%
SW	2.7	84.4	3.3	0.6
SWF-2/1	3.6	78.3	2.6	0.3
SWF-1/2	3.3	78.0	2.7	0.5
SWF-1/4	3.8	80.0	2.4	0.3
SWF-1/8	2.0	69.5	2.6	0.9

of the most important factors affecting the electrocatalytic performance of these catalysts.

As shown in Fig. 6, the sample without PTFE presented Type I adsorption-desorption isotherms, and the BET surface area increased with the temperature. When the temperature reached 900 ℃, the sample had the highest specific surface area (1033.9 $cm^2 \cdot g^{-1}$) (Fig. 6A). Fig. 6B presents the pore size distribution curves derived from the adsorption branch of the isotherms using the density functional theory (DFT) method. All the samples without PTFE displayed noticeable micropores with a pore size of 1.2 nm.

The nitrogen adsorption-desorption isothermal curves of the samples containing PTFE are quite different from the curve of the sample without PTFE (Fig. 6C). Type IV sorption isotherms were obtained for these samples and indicated the generation of mesopores.

From the pore size distribution curves we can see that a large number of mesoporous structures (5 ~ 30 nm in diameter) were generated after the addition of PTFE (Fig. 6D). The micropores and mesopores within the resulting carbon framework of the SWF samples probably arose from the burn-off of many non-carbon and carbon-containing compounds inherent in the biomass, as well as the decomposition of PTFE during pyrolysis. According to the literature, a mesoporous structure is advantageous for mass transfer, which can, in turn, enhance catalytic performance.

RDE measurements were performed to investigate the catalysts' ORR activities. Fig. 7A shows the LSV curves for the catalysts without PTFE. Evidently, their performance was strongly affected by the pyrolysis temperature. The ORR activity increased with

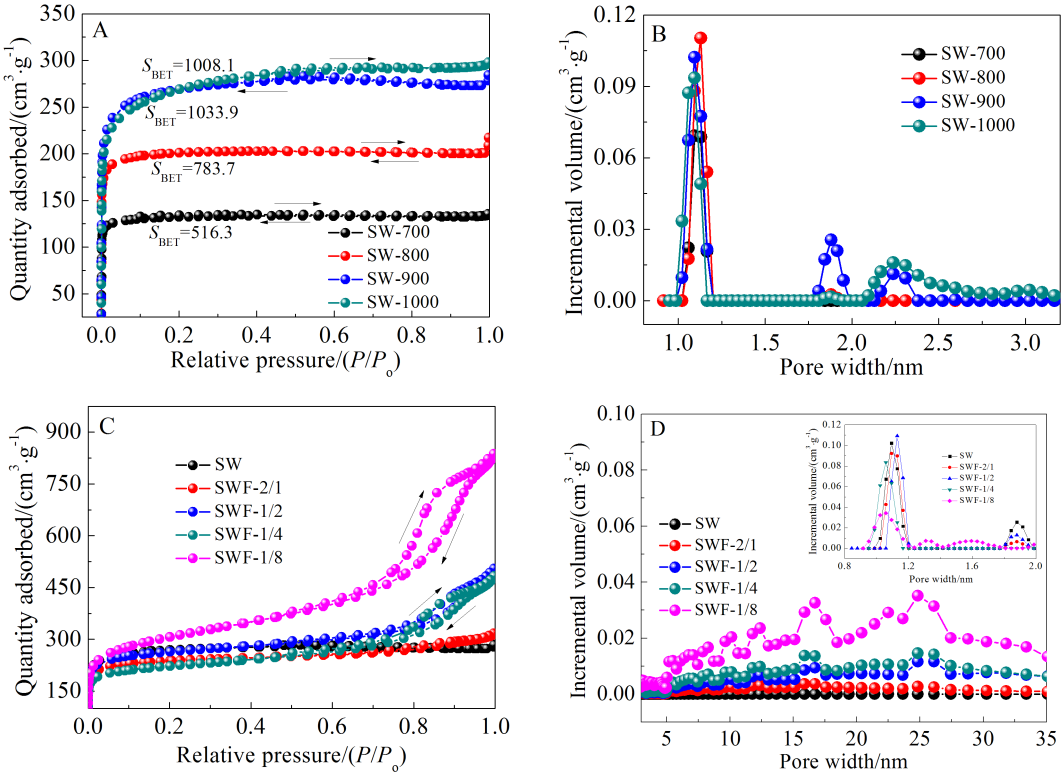

Fig. 6 A-C. N_2 sorption isotherms; B-D. DFT pore size distributions of different samples

temperature, peaking at 900 ℃. It was interesting that this variation of ORR performance with temperature was consistent with the BET surface area results. We therefore will choose 900 ℃ as the optimum temperature in our next experiments.

The addition of PTFE significantly enhanced the catalysts' ORR performance. Compared to the SW catalyst without PTFE, the onset potentials underwent a gradual positive shift as the amount of PTFE increased. SWF-1/4 had a limited current density and current density at 0.78 V up to 4.77 and 5.80 mA·cm^{-2}, respectively-increases of 2.75 and 2.60 mA·cm^{-2} compared with 2.02 and 3.20 mA·cm^{-2} for the SW catalyst. Furthermore, the half-wave potential (0.84 V) and onset potential (0.99 V) of SWF-1/4 exceeded those of 20% Pt/C. In other words, the SWF-1/4 exhibited superior ORR catalytic activity to commercial Pt/C in an alkaline medium.

To understand the ORR kinetics of SWF-1/4, we carried out Tafel analysis. Generally, for a Pt/C

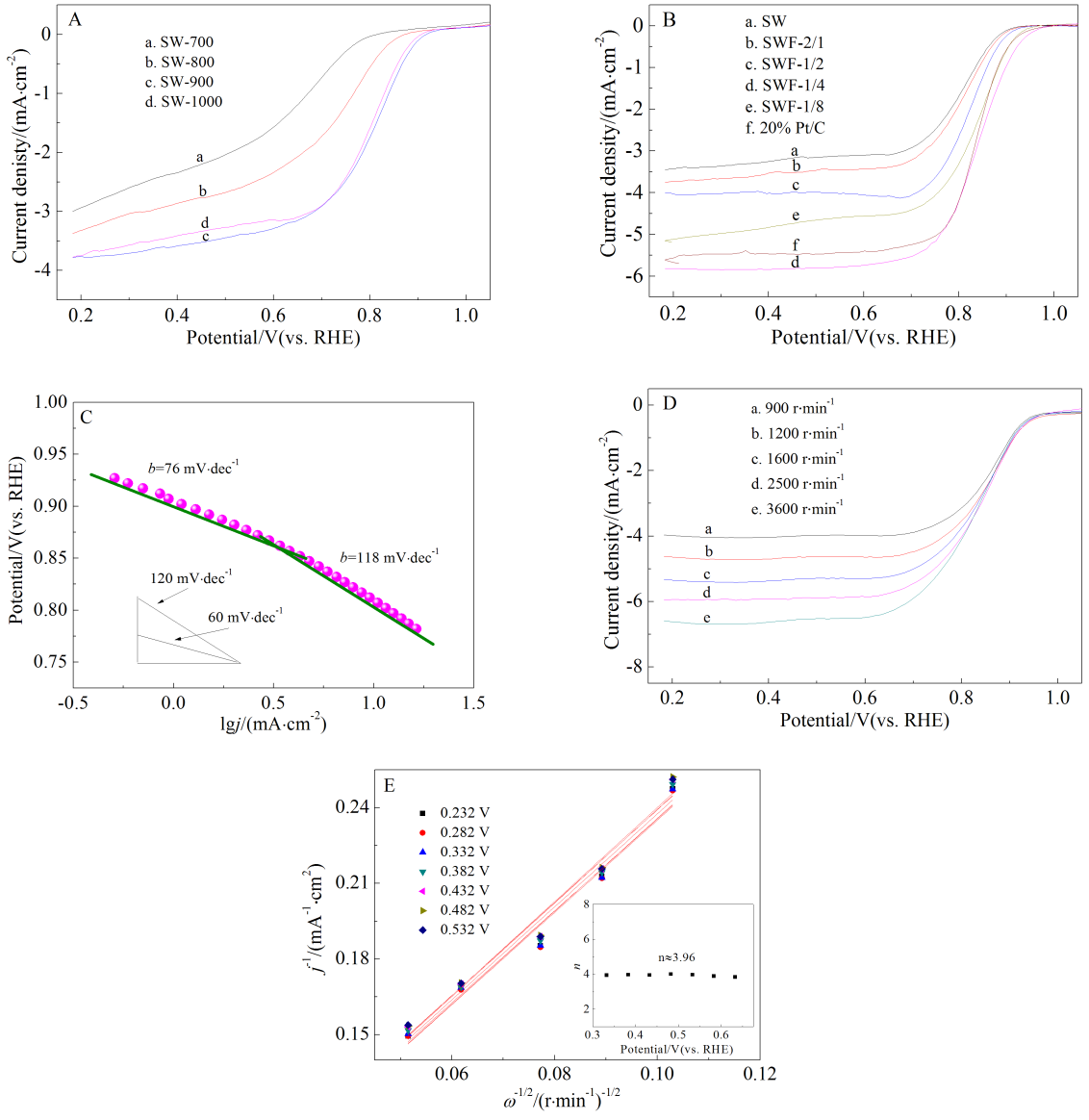

Fig. 7 A. LSV curves for the ORR on samples of pyrolyzed silk cocoon used directly, without added PTFE, at different temperatures after hydrothermal treatment; B. LSV curves for the ORR on different samples pyrolyzed at 900 ℃ in O_2-saturated 0.1 mol·L^{-1} KOH solution; C. Tafel plot; D. Current-potential curves at various rotation rates; E. Koutecky-Levich plots for the ORR on SWF-1/4 electrode using data derived from D (the inset shows the dependence of n on potential)

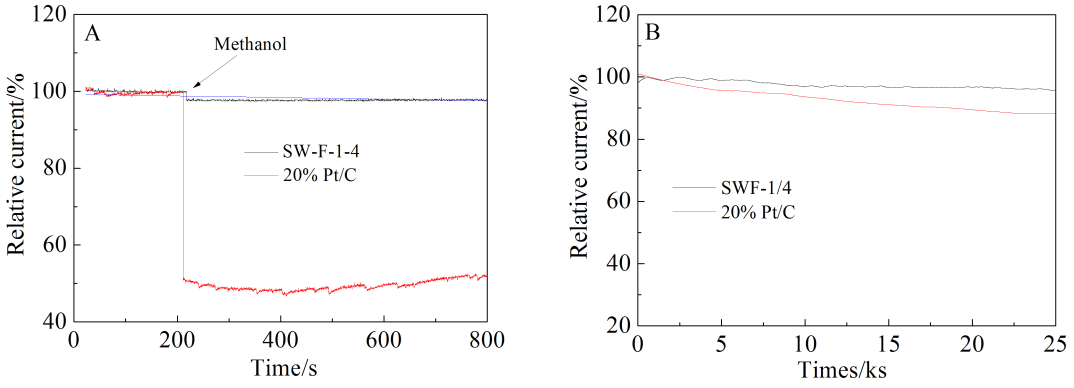

Fig. 8 A. Methanol tolerance tests of SWF-1/4 and Pt/C using chronoamperometric responses at 0.68 V in 0.1 mol·L^{-1} KOH aqueous electrolyte (the arrow indicates the introduction of methanol); B. Long-term durability tests of SWF-1/4 and Pt/C catalysts using current-time chronoamperometric measurements at 0.68 V in O_2-saturated 0.1 mol·L^{-1} KOH solution

catalyst, a Tafel slope value of 120 mV·dec^{-1} at low potentials suggests that the ORR rate is determined by the transfer of the first electron, while at high potentials, a Tafel slope of 60 mV·dec^{-1} is likely due to the migration of adsorbed oxygen intermediates, which becomes the rate-determining step[7, 57-58]. In our Tafel plot (Fig. 7C), the slopes for the SWF-1/4 catalyst are 76 and 118 mV·dec^{-1} at high and low potentials, respectively. These results suggest that the ORR on the SWF-1/4 catalyst may follow the same mechanism as that of Pt/C.

We also plotted the RDE current-potential curves of SWF-1/4 at various rotation speeds (Fig. 7D). Calculated from the slope of the K-L plots, the average number of electrons transferred per O_2 molecule for SWF-1/4 during the ORR was about 3.96 in the potential range of 0.23 ~ 0.53 V (Fig. 7E). These results demonstrate that the ORR process on SWF-1/4 predominantly followed a 4e pathway.

Finally, our catalysts also exhibited excellent methanol tolerance, as shown in Fig. 8A. When methanol was introduced into the testing cell, the current response of SWF-1/4 remained unchanged, indicating its excellent tolerance to methanol poisoning. In contrast, Pt/C exhibited an instantaneous current jump upon the addition of methanol, reflecting its low tolerance. The excellent tolerance of SWF-1/4 makes it a promising cathode catalyst for direct methanol fuel cells, in which methanol tolerance at the cathode is essential due to the trans-membrane crossover of methanol from the anode to the cathode.

The durability/stability of an ORR electrocatalyst is rightly regarded as one of the most important issues to be addressed for practical applications and commercialization; we accordingly assessed SWF-1/4. Fig. 8B shows the current-time (*i-t*) chronoamperometric responses of the SWF-1/4 and Pt/C electrodes at 0.68 V (vs. RHE) in O_2-saturated 0.1 mol·L^{-1} KOH solution at a rotation rate of 900 r·min^{-1}. After 25,000 seconds, the ORR current density of SWF-1/4 decreased by only 4.0%, while that of Pt/C dropped by 15%, indicating that the former exhibited excellent stability.

3 Conclusions

In this work, we demonstrated that a high-performance ORR catalyst could be prepared by pyrolyzing silkworm cocoon biomass and enhancing it with the addition of PTFE. The inherent nitrogen of the raw silk cocoon was efficiently retained in the end product (up to ca. 4%). The PTFE allowed F atoms to be doped into the carbon lattice, which enhanced the ORR activity of the catalyst. This type of biomass-derived catalyst exhibited outstanding electrocatalytic activity, excellent tolerance to methanol poisoning, and superior stability to Pt/C. Thus, this novel catalytic material derived from silkworm cocoon may prove to be an inexpensive, metal-free, and efficient catalyst towards the ORR in fuel cells and, indeed, for applications in other fields.

References:

[1] Steele B C, Heinzel A. Materials for fuel-cell technologies [J]. Nature, 2001, 414(6861): 345-352.

[2] Wang C, Daimon H, Onodera T, et al. A general approach to the size-and shape-controlled synthesis of platinum nanoparticles and their catalytic reduction of oxygen[J]. Angewandte Chemie International Edition, 2008, 47(19): 3588-3591.

[3] Debe M K. Electrocatalyst approaches and challenges for automotive fuel cells[J]. Nature, 2012, 486(7401): 43-51.

[4] Cao R, Thapa R, Kim H, et al. Promotion of oxygen reduction by a bio-inspired tethered iron phthalocyanine carbon nanotube-based catalyst[J]. Nature Communications, 2013, 4: No. 2076.

[5] Li Y G, Gong M, Liang Y Y, et al. Advanced zinc-air batteries based on high-performance hybrid electrocatalysts [J]. Nature Communications, 2013, 4: No. 1805.

[6] Levy R, Boudart M. Platinum-like behavior of tungsten carbide in surface catalysis[J]. Science, 1973, 181(4099): 547-549.

[7] Wu G, More K L, Johnston C M, et al. High-performance electrocatalysts for oxygen reduction derived from polyaniline, iron, and cobalt[J]. Science, 2011, 332(6028): 443-447.

[8] Nie Y, Li L, Wei Z D. Recent advancements in Pt and Pt-free catalysts for oxygen reduction reaction[J]. Chemical Society Reviews, 2015, 44(8): 2168-2201.

[9] Dai L M, Xue Y H, Qu L T, et al. Metal-free catalysts for oxygen reduction reaction[J]. Chemical Reviews, 2015, 115 (11): 4823-4892.

[10] Higgins D, Zamani P, Yu A, et al. The application of graphene and its composites in oxygen reduction electrocatalysis: A perspective and review of recent progress[J]. Energy & Environmental Science, 2016, 9(2): 357-390.

[11] Peng H L, Mo Z Y, Liao S J, et al. High performance Fe- and N-doped carbon catalyst with graphene structure for oxygen reduction[J]. Scientific Reports, 2013, 3: No. 1765.

[12] Mo Z Y, Zheng R P, Peng H L, et al. Nitrogen-doped graphene prepared by a transfer doping approach for the oxygen reduction reaction application[J]. Journal of Power Sources, 2014, 245: 801-807.

[13] You C H, Liao S J, Li H L, et al. Uniform nitrogen and sulfur co-doped carbon nanospheres as catalysts for the oxygen reduction reaction[J]. Carbon, 2014, 69: 294-301.

[14] Zhao Y, Yang L, Chen S, et al. Can boron and nitrogen co-doping improve oxygen reduction reaction activity of carbon nanotubes?[J]. Journal of the American Chemical Society, 2013, 135(4): 1201-1204.

[15] Xue Y H, Yu D S, Dai L M, et al. Three-dimensional B, N-doped graphene foam as a metal-free catalyst for oxy gen reduction reaction[J]. Physical Chemistry Chemical Physic, 2013, 15(29): 12220-12226.

[16] Xu J X, Dong G F, Jin C H, et al. Sulfur and nitrogen co-doped, few-layered graphene oxide as a highly efficient electrocatalyst for the oxygen-reduction reaction[J]. ChemSusChem, 2013, 6(3): 493-499.

[17] Liu Z, Nie H G, Yang Z, et al. Sulfur-nitrogen co-doped three-dimensional carbon foams with hierarchical pore structures as efficient metal-free electrocatalysts for oxy gen reduction reactions[J]. Nanoscale, 2013, 5(8): 3283-3288.

[18] Li R, Wei Z d, Gou X L, et al. Phosphorus-doped graphene nanosheets as efficient metal-free oxygen reduction electrocatalysts[J]. RSC Advances, 2013, 3(25): 9978-9984.

[19] Yang D S, Bhattacharjya D, Inamdar S, et al. Phosphorus-doped ordered mesoporous carbons with different lengths as efficient metal-free electrocatalysts for oxygen reduction reaction in alkaline media[J]. Journal of the American Chemical Society, 2012, 134(39): 16127-16130.

[20] Choi C H, Park S H, Woo S I. Phosphorus-nitrogen dual doped carbon as an effective catalyst for oxygen reduction reaction in acidic media: Effects of the amount of P-doping on the physical and electro chemical properties of carbon[J]. Journal of Materials Chemistry, 2012, 22(24): 12107-12115.

[21] Liu Z W, Peng F, Wang H J, et al. Phosphorus-doped graphite layers with high electrocatalytic activity for the O_2 reduction in an alkaline medium[J]. Angewandte Chemie-International Edition, 2011, 50(14): 3257-3261.

[22] Yang L J, Jiang S J, Zhao Y, et al. Boron-doped carbon nanotubes as metal-free electrocatalysts for the oxygen reduction reaction[J]. Angewandte Chemie-International Edition, 2011, 50(31): 7132-7135.

[23] Gong K P, Du F, Xia Z H, et al. Nitrogen-doped carbon nanotube arrays with high electrocatalytic activity for oxygen reduction[J]. Science, 2009, 323(5915): 760-764.

[24] Wang Y, Nie Y, Ding W, et al. Unification of catalytic oxygen reduction and hydrogen evolution reactions: Highly dispersive Co nanoparticles encapsulated inside Co and nitrogen co-doped carbon [J]. Chemical Communications, 2015, 51(43): 8942-8945.

[25] Guo L, Jiang W J, Zhang Y, et al. Embedding Pt nanocrystals in N-doped porous carbon/carbon nanotubes toward highly stable electrocatalysts for the oxygen reduction reaction[J]. ACS Catalysis, 2015, 5(5): 2903-2909.

[26] Ding W, Li L, Xiong K, et al. Shape fixing via salt recrystallization: A morphology-controlled approach to convert

nanostructured polymer to carbon nanomaterial as a highly active catalyst for oxygen reduction reaction[J]. Journal of the American Chemical Society, 2015, 137 (16): 5414-5420.

[27] Raymundo-Piñero E, Cadek M, Béguin F. Tuning carbon materials for supercapacitors by direct pyrolysis of seaweeds [J]. Advanced Functional Materials, 2009, 19(7): 1032-1039.

[28] Wang X R, Li X L, Zhang L, et al. N-doping of graphene through electrothermal reactions with ammonia[J]. Science, 2009, 324(5928): 768-771.

[29] Zhao L, Fan L Z, Zhou M Q, et al. Nitrogen-containing hydrothermal carbons with superior performance in super capacitors[J]. Advanced Materials, 2010, 22(45): 5202-5206.

[30] Zhu H, Wang X L, Yang F, et al. Promising carbons for supercapacitors derived from fungi[J]. Advanced Materials, 2011, 23(24): 2745-2748.

[31] Falco C, Sevilla M, White R J, et al. Renewable nitrogen-doped hydrothermal carbons derived from microalgae[J]. ChemSusChem, 2012, 5(9): 1834-1840.

[32] Wang K L, Wang H, Ji S, et al. Biomass-derived activated carbon as high-performance non-precious electrocatalyst for oxygen reduction[J]. RSC Advances, 2013, 3(30): 12039-12042.

[33] Ren Y M, Zhang J M, Xu Q, et al. Biomass-derived three-dimensional porous N-doped carbonaceous aerogel for efficient supercapacitor electrodes[J]. RSC Advances, 2014, 4(45): 23412-23419.

[34] Zhang B, Xiao M, Wang S J, et al. Novel hierarchically porous carbon materials obtained from natural biopolymer as host matrixes for lithium-sulfur battery applications[J]. ACS Applied Materials & Interfaces, 2014, 6(15): 13174-13182.

[35] Adinaveen T, Kennedy L J, Vijaya J J, et al. Studies on structural, morphological, electrical and electrochemical properties of activated carbon prepared from sugarcane bagasse[J]. Journal of Industrial and Engineering Chemistry, 2013, 19(5): 1470-1476.

[36] Zhang H M, Wang Y, Wang D, et al. Hydrothermal Transformation of dried grass into graphitic carbon-based high performance electrocatalyst for oxygen reduction reaction[J]. Small, 2014, 10(16): 3371-3378.

[37] Zhai Y L, Zhou C Z, Wang E K, et al. Energetic carbon-based hybrids: Green and facile synthesis from soy milk and extraordinary electrocatalytic activity towards ORR [J]. Nanoscale, 2014, 6(5): 2964-2970.

[38] Song M Y, Park H Y, Yang D S, et al. Seaweed-derived heteroatom-doped highly porous carbon as an electrocatalyst for the oxygen reduction reaction[J]. ChemSusChem, 2014, 7(6): 1755-1763.

[39] Chen P, Wang L K, Wang G, et al. Nitrogen-doped nanoporous carbon nanosheets derived from plant biomass: An efficient catalyst for oxygen reduction reaction[J]. Energy & Environmental Science, 2014, 7(12): 4095-4103.

[40] Gao S Y, Chen Y L, Fan H, et al. Large scale production of biomass-derived N-doped porous carbon spheres for oxygen reduction and supercapacitors[J]. Journal of Materials Chemistry A, 2014, 2(10): 3317-3324.

[41] Lu J, Bo X J, Wang H, et al. Nitrogen-doped ordered mesoporous carbons synthesized from honey as metal-free catalyst for oxygen reduction reaction[J]. Electrochimica Acta, 2013, 108: 10-16.

[42] Liu F F, Peng H L, Qiao X C, et al. High-performance doped carbon electrocatalyst derived from soybean biomass and promoted by zinc chloride[J]. International Journal of Hydrogen Energy, 2014, 39(19): 10128-10134.

[43] Liu F F, Peng H L, You C H, et al. High-performance doped carbon catalyst derived from nori biomass with melamine promoter[J]. Electrochimica Acta, 2014, 138: 353-359.

[44] Liang Y R, Wu D C, Fu R W. Carbon microfibers with hierarchical porous structure from electrospun fiber-like natural biopolymer[J]. Scientific Reports, 2013, 3: No. 1119.

[45] Peng H L, Liu F F, Qiao X C, et al. Nitrogen and fluorine co-doped carbon catalyst with high oxygen reduction performance, prepared by pyrolyzing a mixture of melamine and PTFE[J]. Electrochimica Acta, 2015, 182: 963-970.

[46] Sun X J, Zhang Y W, Song P, et al. Fluorine-doped carbon blacks: Highly efficient metal-free electrocatalysts for oxygen reduction reaction[J]. ACS Catalysis, 2013, 3 (8): 1726-1729.

[47] Nakajima T, Koh M, Gupta V, et al. Electrochemical behavior of graphite highly fluorinated by high oxidation state complex fluorides and elemental fluorine[J]. Electrochim. Acta, 2000, 45(10): 1655-1661.

[48] Zhong M, Kim E K, Mcgann J P, et al. Electrochemically active nitrogen-enriched nanocarbons with well-defined morphology synthesized by pyrolysis of self-assembled block copolymer[J]. Journal of the American Chemical Society, 2012, 134(36): 14846-14857.

[49] Yang S B, Zhi L J, Tang K, et al. Efficient synthesis of heteroatom (N or S)-doped graphene based on ultrathin graphene oxide-porous silica sheets for oxygen reduction reactions[J]. Advanced Functional Materials, 2012, 22

(17): 3634-3640.

[50] Lee D H, Lee W J, Lee W J, et al. Theory, synthesis, and oxygen reduction catalysis of Fe-porphyrin-like carbon nanotube[J]. Physical Review Letters, 2011, 106(17): 175502.

[51] Chen Z, Higgins D, Chen Z W. Nitrogen doped carbon nanotubes and their impact on the oxygen reduction reaction in fuel cells[J]. Carbon, 2010, 48(11): 3057-3065.

[52] Choi C H, Park S H, Woo S I. Phosphorus-nitrogen dual doped carbon as an effective catalyst for oxygen reduction reaction in acidic media: Effects of the amount of P-doping on the physical and electrochemical properties of carbon[J]. Journal of Materials Chemistry, 2012, 22(24): 12107-12115.

[53] Xu Z, Gao C. Graphene chiral liquid crystals and macroscopic assembled fibres[J]. Nature Communications, 2011, 2: 571-579.

[54] White R J, Yoshizawa N, Antonietti M, et al. A sustainable synthesis of nitrogen-doped carbon aerogels [J]. Green Chemistry, 2011, 13(9): 2428-2434.

[55] Chandra V, Yu S U, Kim S H, et al. Highly selective CO_2 capture on N-doped carbon produced by chemical activation of polypyrrole functionalized graphene sheets [J]. Chemical Communications, 2012, 48(5): 735-737.

[56] Ando T, Tanaka J, Ishii M, et al. Diffuse reflectance Fourier-transform infrared study of the plasma-fluorination of diamond surfaces using a microwave discharge in CF_4[J]. Journal of the Chemical Society-Faraday Transactions, 1993, 89(16): 3105-3109.

[57] Wu G, Nelson M, Ma S, et al. Synthesis of nitrogen-doped onion-like carbon and its use in carbon-based CoFe binary non-precious-metal catalysts for oxygen-reduction [J]. Carbon, 2011, 49(12): 3972-3982.

[58] Xiao H, Shao Z G, Zhang G, et al. Fe-N-carbon black for the oxygen reduction reaction in sulfuric acid[J]. Carbon, 2013, 57: 443-451.

蚕茧衍生的氮氟共掺杂碳基催化剂在碱性介质中的氧还原电催化性能的研究

刘芳芳[1,2],彭洪亮[1],廖世军[1*]

(1. 华南理工大学化学化工学院, 广州 510641; 2. 潍坊科技学院化工与环境学院, 山东 寿光 262700)

摘　要:本文通过水热预处理,利用热解工艺从蚕茧中成功地制备了一种高性能的掺杂碳基催化剂. 研究了制备条件及氟原子掺杂对催化剂性能的影响. 在最优化条件下制备出的氮氟共掺杂碳基催化剂具有超过 1000 $m^2 \cdot g^{-1}$ 的比表面积,N 元素和 F 元素含量可达 3.5%及 7.3%. 在碱性条件下, 所制备的催化剂具有可与商业铂碳催化剂相媲美的氧还原催化活性,同时展示出优异的抗甲醇中毒性能及稳定性. F 原子的掺杂对催化剂性能的提高效果显著.

关键词:生物质衍生;氧还原反应;碳材料;氮氟共掺杂